EUROPEAN JOURNAL OF BIOMEDICAL AND PHARMACEUTICAL SCIENCES
http://www.ejbps.com

ISSN 2349-8870
Volume: 12
Issue: 6
Year: 2025

IN-VITRO AND IN-SILICO EVALUATION OF A NOVEL INDENOIMIDAZOLE DERIVATIVE IN A MOUSE MODEL

Ehigie Leonard O[a], Olaniyan Lamidi W. B.*[a,c], Olatomide Fadare[b], Ehigie Adeola F[a], Alabi Olubunmi T[a], Ojeniyi Fiyinfoluwa D[a] and Onikepo Adesina A[a]

[a]Department of Biochemistry, Ladoke Akintola University of Technology, Ogbomoso, Oyo State, Nigeria.
[b]Department of Chemistry, Obafemi Awolowo University, Ile-Ife Osun State, Nigeria.

***Corresponding Author: Olaniyan Lamidi W. B.**
Department of Biochemistry, Ladoke Akintola University of Technology, Ogbomoso, Oyo State, Nigeria.

Article Received on 13/04/2025 **Article Revised on 03/05/2025** **Article Published on 23/05/2025**

ABSTRACT
Malaria remains a major public health issue in tropical and subtropical regions, exacerbated by the rapid emergence of drug-resistant *Plasmodium* species. This study aimed to develop a novel antimalarial agent by investigating a synthesized indenoimidazole derivative as a potential transketolase inhibitor, a key enzyme in the pentose phosphate pathway. The research sought to provide a new avenue for antimalarial therapy. (E)-3a,8a-dihydroxy-3-((2,4-hydroxybenzylidene)amino)-2-thioxo-1,3,3a,8a-tetrahydroindeno[1,2-d] imidazol-8(2H)-one, was synthesized and characterized using IR and NMR spectroscopy. Molecular docking (AutoDock Vina) and molecular dynamics (MD) simulations (GROMACS) assessed the compound's binding affinity and stability with *Plasmodium* transketolase. In-vivo studies evaluated antimalarial efficacy using *Plasmodium berghei*-infected mice, with chemosuppression assays and survival index measurements conducted at doses of 5, 10, and 25 mg/kg. Results indicated absorption band in IR (3344.71 cm^{-1}) and chemical shifts in ^1H NMR confirming the compound's structure. Docking studies showed a binding affinity of -7.8 kcal/mol compared to -6.7 kcal/mol for thiamine pyrophosphate. MD simulations revealed a stable protein-ligand complex with RMSD ~0.2 nm over 50 ns. In-vivo tests showed 85.12% chemosuppression and 100% survival index at 25 mg/kg, outperforming chloroquine (66.58% chemosuppression, 68.97% survival). In conclusion, the indenoimidazole derivative demonstrated strong binding affinity, stability, and significant in-vivo antimalarial activity, suggesting its potential as a transketolase inhibitor. Future research should focus on pharmacokinetics optimization and clinical trials to confirm its efficacy and safety.

KEYWORDS: Indenoimidazole derivative, antimalarial activity, transketolase inhibitor, molecular docking, chemosuppression, *Plasmodium berghei*.

INTRODUCTION
Malaria remains one of the most pressing global health challenges, particularly in sub-Saharan Africa, South-East Asia, and South America. In 2021, approximately 247 million cases were reported globally, with Nigeria bearing the largest share of both cases and fatalities.[1] Caused by protozoan parasites of the *Plasmodium* genus, malaria is transmitted through the bite of an infected female *Anopheles* mosquito. *Plasmodium falciparum*, the deadliest of the five *Plasmodium* species infecting humans, accounts for over 90% of malaria-related deaths, particularly affecting vulnerable groups such as children under five and pregnant women.[2] Beyond its devastating human toll, malaria imposes significant economic burdens on affected regions, perpetuating cycles of poverty through lost productivity and strained healthcare system.[3]

Efforts to combat malaria have been hindered by the growing resistance of *P. falciparum* to existing antimalarial drugs, including chloroquine and artemisinin-based combination therapies (ACTs), which are the current first-line treatment.[4]

Resistance to ACTs, particularly in South-East Asia and parts of Africa, poses a grave threat to global malaria control efforts. This has necessitated a shift towards the development of novel therapies targeting new biological pathways within the parasite.[5] One promising approach is targeting the metabolic pathways critical for parasite survival, such as the pentose phosphate pathway (PPP), which provides essential metabolites and protects against oxidative damage. Transketolase, a key enzyme in the PPP, has emerged as a potential target due to its role in nucleotide synthesis and redox balance.[6] In the search for new antimalarial agents, heterocyclic compounds

have gained attention for their versatility and broad biological activities. Among these, indenoimidazole derivatives, which combine the structural features of indene and imidazole, show significant potential. These compounds interact strongly with enzyme active sites through hydrogen bonding and π-π stacking, making them suitable candidates for enzyme inhibition.[7] The unique chemical and biological properties of indenoimidazole derivatives, combined with their ease of functionalization, position them as promising scaffolds for the development of antimalarial drugs targeting transketolase.[8] Advancements in computational techniques, particularly in-silico methods, have revolutionized the drug discovery process. Molecular docking predicts how a compound fits into the active site of a target protein, while molecular dynamics simulations assess the stability of the protein-ligand complex under physiological conditions.[9]

These computational approaches accelerate drug discovery by identifying promising candidates for further in-vivo testing, such as using murine models to evaluate efficacy in reducing parasitemia and improving survival.[10] Given the urgent need for new antimalarial therapies, this study investigates the potential of a novel indenoimidazole derivative, (E)-3a,8a-dihydroxy-3-((2,4-hydroxybenzylidene)amino)-2-thioxo-1,3,3a,8a-tetrahydroindeno[1,2-d]imidazol-8(2H)-one as a transketolase inhibitor. The compound was designed and synthesized to disrupt the non-oxidative branch of the PPP in P. falciparum. Using a combination of in-silico and in-vivo approaches, the study evaluates the compound's binding affinity and stability with transketolase through molecular docking and dynamics simulations, followed by in-vivo efficacy testing in a murine model of *Plasmodium berghei*. This integrated approach aims to provide insights into developing novel antimalarial therapies capable of overcoming drug resistance.

MATERIALS AND METHOD

Synthesis

All reagents used in the study, including 2,4-dihydroxybenzaldehyde, thiosemicarbazide, ninhydrin, ethanol, and solvents, were of analytical grade and purchased from Sigma-Aldrich. Water was double distilled, and solvents were dried with molecular sieves as necessary. The synthesized compound, (E)-3a, 8a-dihydroxy-3-((2,4-hydroxy benzylidene) amino)-2-thioxo-1,3,3a,8a-tetrahydroindeno[1,2-d] imidazol-8(2H)-one, was characterized by IR and NMR spectroscopy.

Molar equivalents of the 2, 4-dihydroxybenzaldehydes and thiosemicarbazide were added together in a conical flask, 10ml of ethanol was added. The reaction mixture was then irradiated with microwave radiation (pulse) for 60 seconds to get the reactants to dissolve. 3 drops of conc HCl was added to the reaction mixture which afforded a colour change to yellow after which the reaction mixture was irradiated further (30 seconds). At the end of the reaction, the observed colour became more intense. The reaction was monitored with thin layer chromatography. Upon leaving the reaction mixture to stand for a day, pure crystalline solid (product) was observed which was isolated by filtration. Thiosemicarbazone (0.0047mol, 1g) was reacted with ninhydrin (0.0047mol, 0.84g) in a conical flask with 10 ml of ethanol. Few drops of aqueous HCl were added to the reaction mixture which was stirred at room temperature (for 24 hours). It was observed that the colour of the reaction mixture changed from yellow to orange during the course of the reaction. The progress of the reaction was monitored using thin layer chromatography. The reaction mixture was filtered to obtain the orange-coloured product and the melting point obtained.

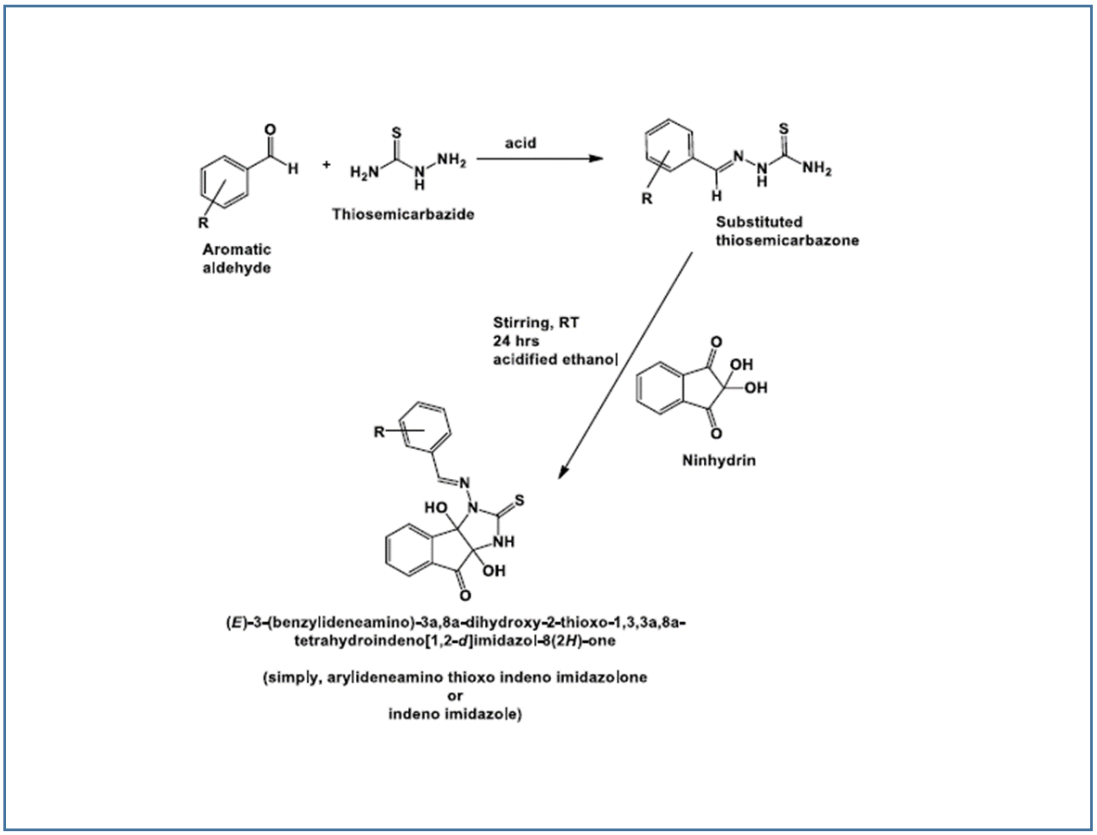

Figure 1: Scheme of synthesis for (E)-3a, 8a-dihydroxy-3-((2, 4-hydroxy benzylidene) amino)-2-thioxo-1, 3, 3a, 8a-tetrahydroindeno [1, 2- d] imidazol-8(2H)-one.

Protein model construction (homology modelling)

The amino acid sequence of the target protein, Plasmodium falciparum transketolase, was obtained in FASTA format from the National Centre for Biotechnology Information (NCBI). To identify a suitable template protein with homology, we conducted a similarity search in the Protein Data Bank (PDB) using the BLASTp tool. The selection of the template protein was based on various factors, including the percentage of homology with the target, the resolution of the 3D structure, and the statistical significance (E-value) of the alignment between the target and template protein. Next, we aligned the amino acid sequence of the target protein with that of the chosen template protein, Saccharomyces cerevisiae transketolase, using the python script "align2d.py" from the MODELLER software to achieve an optimal alignment. Following this, we utilized the python script "Build_profle.py" from the same MODELLER software to generate five similar models.[14] Among these models, we selected the one with the lowest Discreet Optimized Potential Energy (DOPE) and the highest GA341 score as the most suitable model for the *P. falciparum* transketolase. To validate the constructed model, we employed the python script "evaluate_model.py." Additionally, we verified the model's accuracy by generating ramachandran plot through the Zlab server provided by the University of Massachusetts Medical School. Furthermore, we calculated the Root Mean Square Deviation (RMSD) of the modelled protein structure to assess its precision and reliability.

Protein structure optimization

The GROMACS software[15] was employed for the molecular dynamic simulation of the *P. falciparum* transketolase homology model. Initially, a comprehensive topology was generated to define the molecule's attributes for the simulation. The OPLS AA force field was utilized, and a rhombic-dodecahedron box filled with water molecules was employed. Ions were added to neutralize the charges in the solvated protein system.

Following this, the homology model's 3D structure underwent energy minimization to eliminate steric clashes and ensure proper geometry. Subsequently, the solvent and ions surrounding the protein were equilibrated to attain the desired temperature, pressure, and density.

Once the system achieved proper equilibration, the production molecular dynamics phase was initiated to collect data. The simulated protein was then subjected to various analyses, including the assessment of stability using RMSD, as well as the evaluation of the radius of gyration and solvent-accessible surface area. These analyses aimed to characterize the behavior and properties of the simulated protein throughout the molecular dynamic simulation.

Molecular docking

The docking investigations were conducted employing Autodock tools v1.5.4, as described by Morris et al.[16], and AutodockVina v1.1.2, as outlined by Trott and Olson.[17] Chemical structures were constructed using Chemdraw v12.0, and energy minimization was accomplished with Chem 3D v12.0. Subsequently, the molecular docking of the synthesized compound and thiamine pyrophosphate (TPP) was executed. TPP, a crucial cofactor for transketolase, was initially converted from .pdb to. pdbqt format. Following this, its binding site was analyzed and assigned a grid box (search space area) using Autodock Tool. Ligands were prepared for the docking process using Chem3D and Autodock Tools. Subsequent to the preparation of both ligands and protein, Autodock Vina was employed to dock each ligand into the protein, allowing for the estimation of binding affinity and identification of the optimal binding pose.

MD simulation and free energy estimation

Molecular dynamics investigations of protein-ligand interactions were conducted using the GROMACS 2018.3 software, running on an Ubuntu 18.04 LTS platform.[15] The simulation employed the docked structures of the protein-ligand complex. For the protein, pdb2gmx and the GROMOS54a7atb.ff force field obtained from the automated topology builder website were used to prepare the topology file, while the ligand topology file was generated with the Automated Topology Builder (ATB) version 3.0.

To establish the simulation environment, a cubic box containing solvent molecules was added, maintaining a minimum distance of 1.0 nm from the nearest protein atom. The inclusion of Cl- ions helped neutralize the system. Energy minimization was executed with the steepest descent algorithm, involving 50,000 steps and a maximum force threshold of 5 kJ/mol. The simulation incorporated the Verlet cut-off scheme with Particle Mesh Ewald (PME) for managing long-range electrostatic interactions. During the equilibration phase, position restraints were applied. NVT equilibration was conducted at 300 K for 100 ps, followed by NPT equilibration using Parrinello-Rahman pressure coupling at a reference pressure of 1 bar and 100 ps of steps. Bond lengths were constrained using the LINCS algorithm.

Subsequently, a production molecular dynamics simulation of the protein-ligand complex was run for a duration of 50 ns. Following the simulation, various structural parameters, including the RMSD of backbone residues, the count of Hydrogen bonds, Root Mean Square Fluctuations (RMSF), Radius of Gyration (RG), and Solvent Accessible Surface Area (SASA), were computed.[18]

For estimating the free energy of binding between the ligands and the modeled transketolase, the g_mmpbsa protocol, tailored for the GROMOS96 43a1 force field, was employed. The Molecular Mechanics Poisson-Boltzmann Surface Area (MM-PBSA) method, a widely accepted approach, was used to forecast the stability of complexes and compute the free binding energy.[19] Notably, the MM-PBSA algorithm is open-source software and has been extensively used as a scoring function in computational drug design.[20]

In this study, the MM-PBSA method was applied to calculate the free energy of binding between the investigated compound, TPP, and the modeled transketolase. The free energy of binding (Gbinding) was determined by subtracting the total free energy of the protein-inhibitor complex (Gcomplex) from the combined free energies of the isolated forms of the protein (Gprotein) and inhibitor (Gligand) in solvent.

$$\mathbf{Gbinding = Gcomplex - (Gprotein + Gligand)}$$

Average binding energy calculations were performed using a python script provided in the g_mmpbsa stand-alone program.

Pharmacological studies

Determination of Acute Toxicity (LD_{50})

Acute toxicity of (E)-3a, 8a-dihydroxy-3-((2, 4-hydroxy benzylidene) amino)-2-thioxo-1, 3, 3a, 8a-tetrahydroindeno [1, 2- d] imidazol-8(2H)-one was determined using the Lorke's method.[21] Nine mice were divided into three groups (A, B, and C). The three groups were administered orally with graded doses (10, 100, 1000 mg/kg respectively) of the compound in a single dose. The animals were closely monitored for 24 hours for any manifestation of toxicity.

Inoculation with Parasite

Swiss albino mouse weighing 18-20 g previously infected with Plasmodium parasite (parasitemia level of 40 %) was used as donor. The donor mouse was sacrificed with chloroform anesthesia and blood was collected into sterile disposable syringe by cardiac puncture method. The desired volume of blood collected from the donor mouse was appropriately diluted with saline based on the calculated percentage parasitemia of the donor mouse. Each experimental mouse was inoculated intraperitoneally with 0.2 ml of the infected blood.

Grouping and Dosing of Animals

Swiss albino mice were randomly divided into five groups (with five mice per group). Three groups were assigned as test groups while the other two groups were used as control (positive and negative) groups. Different doses of the synthesized compound were dissolved in olive oil. The animals in the test groups were administered with doses of 5, 10 and 25 mg/kg of (E)-3a, 8a-dihydroxy-3-((2, 4-hydroxy benzylidene) amino)-2-thioxo-1, 3, 3a, 8a-tetrahydroindeno [1, 2- d] imidazol-8(2H)-one respectively while the control groups were administered with 10 mg/kg chloroquine (reference drug, positive control) and 0.2 ml of vehicle (olive oil) for the negative control group for four consecutive days

Suppressive Test

The chemosuppressive test was evaluated using the Knight and Peters (1980) method against mice infected with chloroquine-sensitive *Plasmodium berghei*. The mice were infected on the first day of the experiment. Twenty-four hours post-infection, the experimental mice were distributed into groups as described in the grouping and dosing section. The synthesized compound was administered for four consecutive days. The percentage parasitemia was determined to evaluate the effectiveness of the compound.

Determination of Parasitemia

The determination of parasitemia was carried out on the fifth day (120 hours post infection). Thin blood smear of each of the mouse was done by taking a drop of blood from a tiny cut to the tail of the animal on to a microscope glass slide and spreading it thinly with the aid of another slide. The smear was air-dried and then fixed with methanol. The glass slide was allowed to dry and was then stained with Giemsa solution (diluted 1:10 with phosphate buffered saline). The stain was sufficiently poured on each of the slide and allowed to stand for 1 hour, decanted, slowly rinsed with water and dried. The slides were viewed under the light microscope (with 100-x magnification, oil immersion) individually. The parasitemia level was determined by counting the number of parasitized red blood cells out of the total red blood cell in random fields of microscope. The percentage chemo suppression of parasitemia for each dose level was calculated by comparing the percentage parasitemia of the controls (positive and negative control) with those of treated mice using the modified Knight and Peters (1980).

$$\% \text{ Parasitemia} = \frac{\text{Parasitized blood cells}}{\text{Total blood cells}} \times 100$$

$$\% \text{ Chemosuppression} = \frac{(A-B)}{A} X100$$

Where "A" is the average parasitemia for the negative control group and "B" is the average parasitemia for the test compounds.

Determination of Survival Index

Daily monitoring of mortality was conducted, with the number of days from parasite inoculation to death recorded for each mouse in both the treatment and control groups during the follow-up period. The survival index, representing the percentage of animals that survived, was calculated after closely observing and tracking the animals until day 28 post-infection in the chemosuppression experiment. The formula used to calculate the survival index is provided below.[23]

$$\text{Survival Index (SI) (\%)} = \frac{A - B}{C - B} \times 100$$

Average number of days that the test group survived = A
Average number of days that the negative control survived = B
Maximum number of days for the test groups = C

RESULTS AND DISCUSSION

Synthesis and Characterization of (E)-3a, 8a-Dihydroxy-3-((2,4-Hydroxybenzylidene) Amino)-2-Thioxo-1,3,3a,8a-Tetrahydroindeno[1,2-d] Imidazol-8(2H)-one

The synthesis of (E)-3a, 8a-dihydroxy-3-((2,4-hydroxybenzylidene) amino)-2-thioxo-1,3,3a,8a-tetrahydroindeno[1,2-d]imidazol-8(2H)-one was successfully carried out in a two-step process. Initially, thiosemicarbazide was condensed with 2,4-dihydroxybenzaldehyde in ethanol with the aid of concentrated hydrochloric acid as a catalyst. This step produced a thiosemicarbazone intermediate, evident from the yellow crystalline precipitate. The intermediate was purified and subsequently subjected to cyclization with ninhydrin in the presence of an acidic medium to form the desired indenoimidazole compound. The final product, isolated as an orange crystalline solid, demonstrated the formation of the expected fused heterocyclic system.

The key structural change during the cyclization process is the loss of molecular symmetry. Prior to cyclization, ninhydrin possesses a high degree of symmetry, with its two carbonyl groups and hydroxyl group arranged symmetrically around the core (as shown in Figure 2a). Upon substitution of ninhydrin with the thiosemicarbazone intermediate, the molecule maintains this symmetry, although now centered around a new chiral carbon bearing the hydroxyl (-OH) and R-group (as depicted in Figure 2b). However, the subsequent cyclization reaction breaks this symmetry due to the formation of the indenoimidazole ring. This disruption of symmetry is clearly illustrated in Figure 2c, where the cyclized structure displays non-equivalent proton environments in the aromatic rings, leading to distinct NMR signals. This structural transformation significantly alters the chemical environment of the molecule, as evidenced by both NMR and IR spectroscopy.

The 1H NMR spectrum of the synthesized compound reveals the disruption of symmetry in the aromatic region. Prior to cyclization, the protons in the ninhydrin moiety are magnetically equivalent, leading to fewer distinct signals. However, after cyclization, the aromatic protons exhibit splitting into distinct multiplets between δ 7.56 and δ 8.40, confirming the loss of symmetry and the formation of the indenoimidazole core. Additionally, the hydroxyl protons resonate at a high chemical shift around δ 12.51, indicating strong hydrogen bonding interactions. The presence of signals at δ 9.43 and δ 8.83 further confirms the formation of the imidazole ring. This splitting pattern is characteristic of a fused heterocyclic system, where the newly formed rings create unique electronic environments for the protons, consistent with previous reports on indenoimidazole derivatives.[24]

Further confirmation of the structural changes was provided by infrared (IR) spectroscopy. The IR spectrum

of the compound shows a broad absorption band at 3343 cm^{-1}, corresponding to the O-H stretching vibrations of the hydroxyl groups. A sharp peak at 1681 cm^{-1} was observed for the C=O stretching vibration, confirming the presence of a carbonyl group within the indenoimidazole structure. Additionally, a peak at 1561 cm^{-1} was assigned to the C=N stretching, characteristic of the imine group formed during the condensation step. The aromatic C=C stretching vibrations were observed around 1233 cm^{-1}, further validating the presence of aromatic rings within the compound. These spectral features are in agreement with the structural changes observed in the NMR analysis and confirm the successful synthesis of the target molecule.[25]

The loss of symmetry during the cyclization process, as depicted in Figure 2c, is crucial for the biological activity of the compound. The rigid, fused ring system of the indenoimidazole provides a stable framework for potential interactions with biological targets, such as enzymes or receptors, and enhances the compound's binding affinity. This structural rigidity, combined with the presence of functional groups such as hydroxyl and imine moieties, positions the synthesized compound as a promising candidate for further biological evaluations, including enzyme inhibition studies and antimalarial assays.

The characterization of the compound through NMR and IR spectroscopy provides strong evidence of its successful synthesis. The observed spectral patterns are consistent with the literature for related indenoimidazole compounds and support the proposed structural transformations. The changes in symmetry, as highlighted in Figure 2, play a pivotal role in the compound's overall stability and reactivity, making it a suitable candidate for further exploration in drug development.[26]

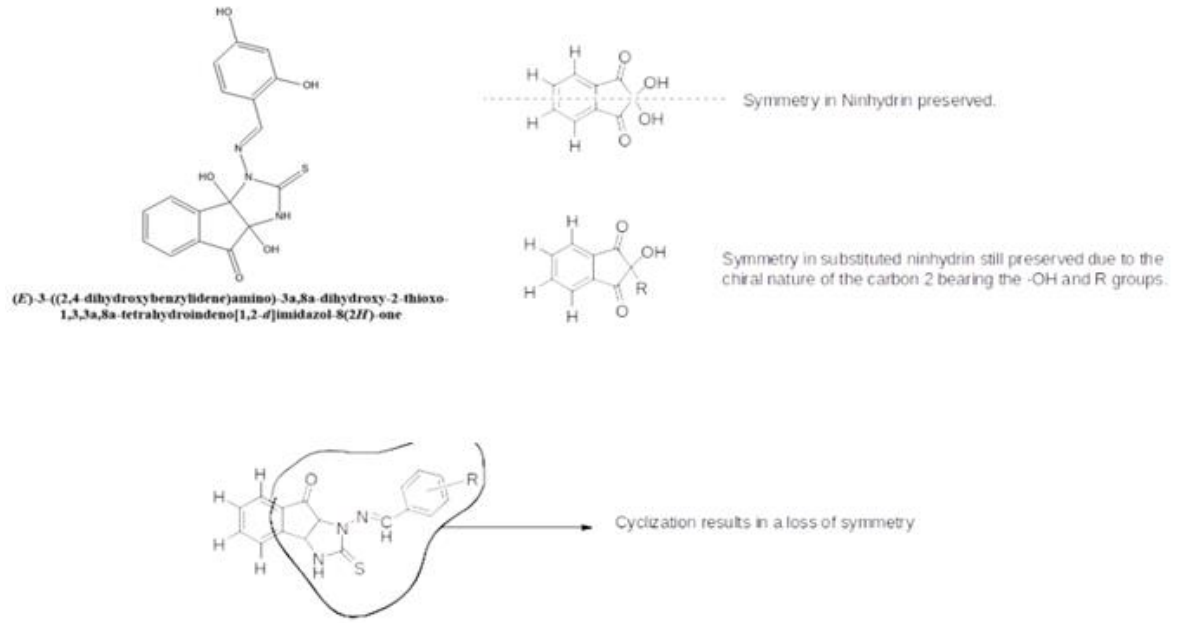

Figure 2: Chemical Structures Showing Symmetry Changes in Ninhydrin and Synthesized Compound. 1a: Chemical structure of the synthesized compound (E)-3a, 8a-dihydroxy-3-((2,4-hydroxybenzylidene) amino)-2-thioxo-1,3,3a,8a-tetrahydroindeno[1,2-d]imidazol-8(2H)-one.
b: Chemical structures showing the presence of symmetry in ninhydrin and substituted ninhydrin prior to cyclization. The symmetric arrangement of functional groups is preserved, even after substitution at carbon.
c: A chemical structure of the synthesized compound illustrating the loss of symmetry after the cyclization of ninhydrin. The newly formed indenoimidazole ring system disrupts the symmetry, resulting in distinct proton environments, as confirmed by NMR and IR analyses.

Table 1: **Spectroscopic and Physicochemical Data of the Synthesized Compound.**

Property	**Data**
Molecular Formula	C17H13N3O4S
Color	Orange
IR (cm^{-1})	O-H: 3343.42; C=O: 1681.03; C=N: 1561.75
^{1}H NMR (500 MHz, DMSO)	δ 12.51 (s, 1H), 9.43 (s, 1H), 8.83 (s, 1H), 8.40–7.56 (m, 13H)

Physicochemical and Spectroscopic Characterization

The physicochemical and spectroscopic properties of the synthesized compound (E)-3a, 8a-dihydroxy-3-((2,4-hydroxybenzylidene)amino)-2-thioxo-1,3,3a,8a-tetrahydroindeno[1,2-d]imidazol-8(2H)-one were characterized extensively. The compound was isolated as an orange crystalline solid with the molecular formula C17H13N3O4S. The melting point of the compound could not be determined under the experimental conditions.

IR Spectroscopy

The infrared (IR) spectrum of the compound was recorded, revealing characteristic absorption peaks (Figure 3a). A broad absorption band at 3343.4 cm^{-1} corresponds to the O-H stretching vibrations of the hydroxyl groups. The C=O stretching vibration of the imidazole ring appears at 1681.8 cm^{-1}, while a sharp peak at 1561.8 cm^{-1} corresponds to the C=N stretching, confirming the presence of an imine bond. Additionally, the aromatic C=C stretching vibrations are observed at 1233.75 cm^{-1}, indicating the presence of aromatic systems in the compound. These key absorption bands confirm the formation of the intended structure.

NMR Spectroscopy

The proton (1H) nuclear magnetic resonance (NMR) spectrum of the compound (Figure 2b) provided further structural confirmation. A singlet at δ 12.51 ppm is attributed to the hydroxyl proton (-OH), which is likely involved in hydrogen bonding. The aromatic protons of the substituted benzylidene moiety give rise to multiplets between δ 8.40 and 7.56 ppm. Additionally, singlet peaks are observed at δ 9.43 ppm and δ 8.83 ppm, corresponding to the protons on the imine (C=N) and the imidazole ring, respectively. The detailed chemical shifts confirm the presence of the indenoimidazole structure in the synthesized compound.

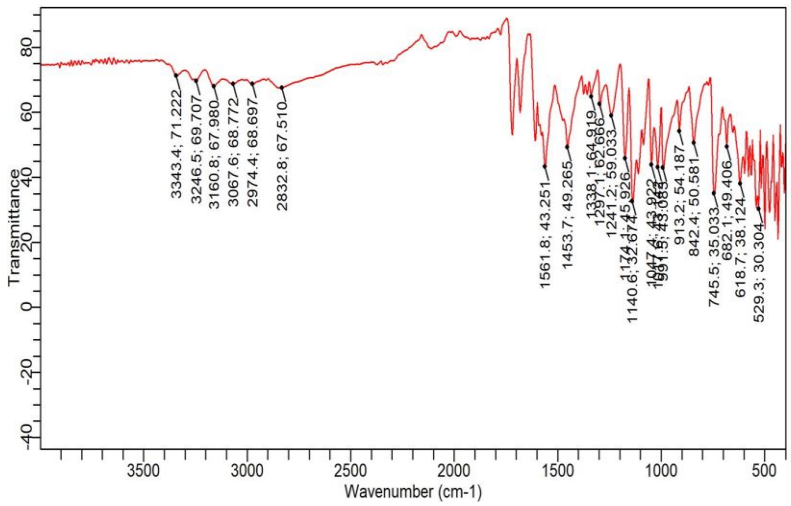

Figure 3A.

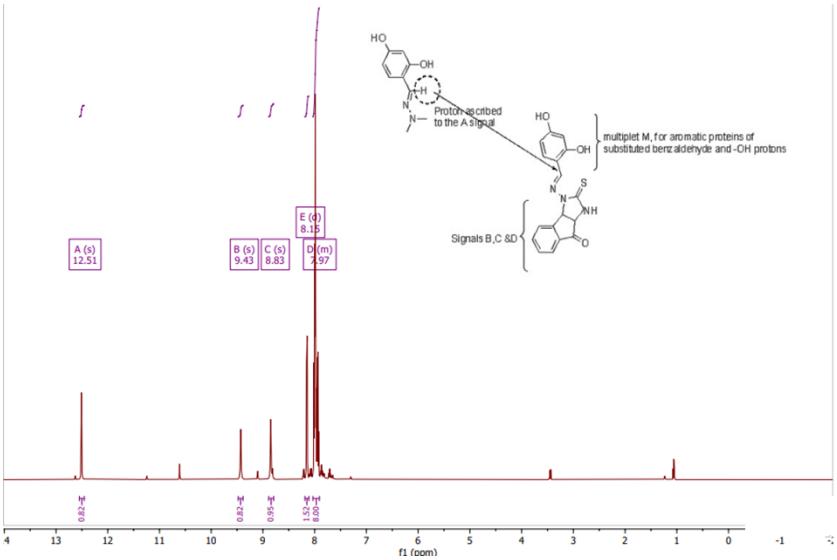

Figure 3B.

Figure 3: Spectroscopic Characterization of (E)-3a, 8a-Dihydroxy-3-((2,4-Hydroxybenzylidene) Amino)-2-Thioxo-1,3,3a,8a-Tetrahydroindeno[1,2-d]Imidazol-8(2H)-one. (A) IR spectrum showing key absorption bands: O-H stretching at 3343.4 cm^{-1}, C=O stretching at 1681.8 cm^{-1}, and C=N stretching at 1561.8 cm^{-1}. (B) ^1H NMR

spectrum showing chemical shifts: δ 12.51 ppm (OH), δ 9.43 ppm (C=N), δ 8.83 ppm (Imidazole protons), and aromatic proton multiplets between δ 8.40 and 7.56 ppm.

Homology Modelling and Structural Evaluation of Plasmodium falciparum Transketolase

Homology modeling is an essential computational method used to predict the three-dimensional structure of proteins, particularly when experimental techniques such as X-ray crystallography or NMR spectroscopy are unavailable. This technique has been widely used for drug discovery and understanding protein function, especially for pathogens like Plasmodium falciparum, where structural information can be critical for identifying therapeutic targets.[27] In this study, the transketolase enzyme from Plasmodium falciparum was modeled using Saccharomyces cerevisiae transketolase (PDB ID: 1GPU) as a template, which showed 48.8% sequence identity and 98% query coverage. These parameters indicate high reliability for modeling the target protein, ensuring that key structural features are preserved, especially those involved in the enzyme's catalytic function.[28]

Transketolase is vital for the parasite's pentose phosphate pathway, a process that maintains redox balance and is crucial for synthesizing nucleotides. Disrupting this enzyme's activity presents a promising strategy for antimalarial drug development.[29] The sequence alignment conducted using Clustal Omega confirmed the conservation of key residues involved in the enzyme's active site, further justifying the choice of Saccharomyces cerevisiae transketolase as the template (Figure 4a). The strong conservation of active site residues is critical because any future efforts to design inhibitors must consider these functional regions to effectively block enzymatic activity.[30]

Five homology models of Plasmodium falciparum transketolase were constructed using MODELLER, a tool known for generating reliable models by incorporating sequence alignment data while minimizing energy to achieve the most stable structure.[28] Out of the five generated models, the one with the lowest Discrete Optimized Protein Energy (DOPE) score of -84453.69531 was selected, as it showed the highest likelihood of representing the native structure of the enzyme. Additionally, the GA341 score of 1.00000 further validated the model, indicating that it is highly reliable and suitable for downstream studies such as molecular docking.[31]

DOPE scores have been widely used to evaluate the overall energy of a protein model, where lower scores reflect a more energetically favorable conformation.[32] The GA341 score, which ranges from 0 to 1, assesses the reliability of the model, with values close to 1.0 suggesting a high-quality model suitable for further structural and functional analysis.[33] These metrics are essential in ensuring that the generated model can be trusted for further studies, especially when used for drug design.[34]

The accuracy of the homology model was further validated by comparing its energy profile to that of the template protein. As shown in Figure 4b, the energy profile of the target protein closely aligns with that of the template, indicating similar structural stability between the two proteins. This is an important step in model validation because it provides insight into how the protein might fold and behave under physiological conditions.[35] Large deviations in the energy profile could indicate potential errors in the model, such as misfolding or incorrect loop modeling, which would render the model unsuitable for drug design.[36] However, the alignment of the energy profiles suggests that the model accurately represents the native fold of Plasmodium falciparum transketolase.

The energy profile is a reflection of the structural integrity of the model, where regions of high energy can signify instability or incorrect folding. The close match between the energy profiles of the model and the template highlights the reliability of the model, making it suitable for subsequent applications such as virtual high-throughput screening and molecular dynamics simulations.[37]

Further structural validation was carried out using a Ramachandran plot, a standard tool for assessing the stereo-chemical quality of protein models (Figure 4c). The plot showed that 84.7% of the residues were in the most favored regions, with an additional 6.37% in allowed regions. Only 4.72% of the residues were in the outlier regions, which is within the acceptable range for homology models.[38] This level of stereo-chemical quality suggests that the model is highly reliable, with only a small proportion of residues adopting conformations that deviate from ideal bond angles.[39]

The importance of the Ramachandran plot lies in its ability to provide insights into the overall geometry of the protein. Residues in outlier regions can often occur in flexible or disordered regions of the protein, such as loops or termini, which are less critical to the protein's overall stability and function.[40] Given the small percentage of outliers in this model, it can be concluded that the protein's core regions, including the active site, are well-modeled and suitable for future studies involving ligand binding and inhibitor design.[41]

The homology model of Plasmodium falciparum transketolase generated in this study offers a robust platform for structure-based drug design. Since transketolase plays a crucial role in the pentose phosphate pathway, inhibiting this enzyme could disrupt the parasite's ability to synthesize nucleotides and

maintain redox balance, thereby impairing its growth and survival.[42] The conserved regions in the enzyme's active site make this model a valuable tool for virtual screening efforts aimed at identifying potential inhibitors.[43]

Additionally, the close energy profile alignment between the model and the template reinforces the structural accuracy of the model. This alignment is particularly important for predicting interactions between the enzyme and small-molecule inhibitors, as an accurate energy profile ensures that the model reflects the enzyme's functional conformation.[44] Furthermore, the high percentage of residues in the favored regions of the Ramachandran plot supports the use of this model in molecular docking and molecular dynamics simulations, both of which are essential for optimizing potential drug candidates.[45]

Given the importance of transketolase in the metabolic processes of *Plasmodium falciparum*, the model generated in this study can be employed in virtual high-throughput screening to identify potential inhibitors. These inhibitors could be developed into antimalarial drugs, providing a novel approach to combating drug-resistant strains of malaria.[46]

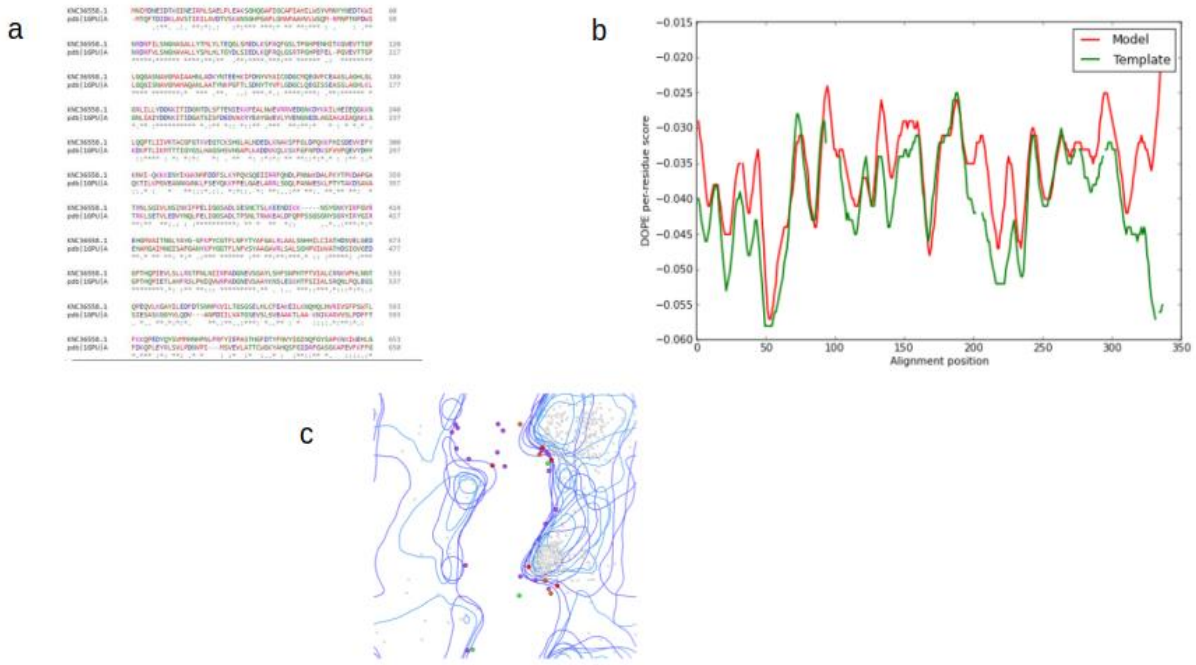

Figure 4: Homology Modelling and Evaluation of Plasmodium falciparum Transketolase. a) Amino acid sequence alignment between Plasmodium falciparum transketolase (KNC36558.1) and Saccharomyces cerevisiae transketolase (PDB ID: 1GPU_A). This alignment shows conserved regions and homology between the target and template proteins. b) Energy profile comparison between the target protein model and the template protein. The alignment in the energy distribution suggests structural stability and close resemblance between the model and template. c) Ramachandran plot of the homology model of Plasmodium falciparum transketolase. Light blue regions indicate highly favored areas, purple regions are allowed areas, and dark regions represent outliers, which account for 4.72% of the residues. This plot confirms the stereo-chemical quality of the model.

Molecular Docking Studies

Molecular docking is an essential computational technique used to predict how small molecules, such as synthesized compounds, interact with their biological targets. In this study, molecular docking was employed to investigate the interactions between (E)-3a, 8a-dihydroxy-3-((2, 4-hydroxybenzylidene) amino)-2-thioxo-1, 3, 3a, 8a-tetrahydroindeno[1, 2- d] imidazol-8(2H)-one and the enzyme transketolase from *Plasmodium falciparum*. The results of this docking study provide critical insights into the potential of the synthesized compound to inhibit the enzyme, offering implications for antimalarial drug development.

Using CASTp to identify the active site of the transketolase enzyme, the docking simulations were carried out within a grid box optimized to include key catalytic residues. The synthesized compound exhibited a binding affinity of -7.8 kcal/mol, indicating a strong interaction with the enzyme's active site (Table 2). This value is particularly noteworthy when compared to the binding affinity of the enzyme's natural cofactor, thiamine pyrophosphate (TPP), which showed a lower affinity of -6.7 kcal/mol.

The higher binding affinity of the synthesized compound compared to TPP suggests that it could potentially act as a competitive inhibitor of transketolase. This is significant because competitive inhibition could

effectively block the enzyme's function, thus disrupting the pentose phosphate pathway, which is crucial for the parasite's nucleotide synthesis and redox homeostasis. A similar study by Nath and Atkins demonstrated that small molecules targeting the active sites of key enzymes in the pentose phosphate pathway could lead to effective parasite inhibition.[47] Our findings support this hypothesis, indicating that the synthesized compound could offer a new mechanism of action against *Plasmodium falciparum* by outcompeting TPP for enzyme binding.

The docking simulation provided detailed insights into the molecular interactions between the synthesized compound and the enzyme. Figure 5a shows the 2D representation of the binding mode of the synthesized compound within the active site of transketolase. Key hydrogen bonds were formed between the carboxyl group (-COO) of GLU 221 and the hydroxyl group (-OH) of the benzene moiety of the ligand, with a bonding distance of 2.2 Å (Table 2). These hydrogen bonds are critical for stabilizing the compound in the enzyme's active site, facilitating a strong and stable interaction.

This interaction is particularly important because GLU 221 is known to play a pivotal role in the catalytic mechanism of transketolase, as previously reported by Nauton et al.[48] Their study highlighted the essentiality of residues such as GLU and ASP in maintaining the enzyme's catalytic activity. Our docking results, showing strong interactions with GLU 221, suggest that the synthesized compound could potentially disrupt the enzyme's catalytic function, thereby impairing its activity.

Interestingly, the synthesized compound's binding affinity is higher than that of TPP, despite the latter also forming significant interactions with catalytic residues such as HIS 31, GLY 161, and ASP 160 (Figure 5b). However, as shown in Table 2, the bonding distances for TPP (ranging from 1.8 Å to 3.3 Å) are slightly longer and involve weaker interactions compared to the synthesized compound. These findings suggest that while TPP interacts with key catalytic residues, the synthesized compound forms more stable and energetically favorable interactions. This is consistent with the work of Ali et al.[49] who demonstrated that synthetic inhibitors with shorter hydrogen bond distances often exhibit stronger inhibitory effects on enzyme activity.

The docking results suggest that the synthesized compound could effectively inhibit the activity of transketolase by displacing TPP, thus blocking the enzyme's catalytic function. This is particularly important because transketolase plays a crucial role in the pentose phosphate pathway, which is vital for maintaining the redox balance and nucleotide biosynthesis in Plasmodium falciparum. Inhibition of this pathway could lead to parasite death, offering a promising therapeutic strategy against malaria.

Moreover, the strong interaction between the synthesized compound and GLU 221 (as shown in Figure 5a) may have broader implications for drug design. According to Jung et al.[50] inhibitors targeting key residues in metabolic enzymes are often highly effective in disrupting enzyme activity. Our findings align with this, suggesting that future drug design efforts could focus on developing compounds that target similar residues to enhance binding affinity and inhibitory potential.

Additionally, the fact that the synthesized compound exhibits a stronger binding affinity than TPP (Table 2) is an encouraging result for its potential as an antimalarial agent. This is particularly relevant in the context of growing resistance to traditional antimalarial drugs, such as artemisinin-based therapies. The ability of the synthesized compound to bind more strongly than the natural cofactor suggests it could be developed into a potent inhibitor capable of overcoming existing resistance mechanisms.

The findings from this study are consistent with previous research that has identified transketolase as a viable drug target in Plasmodium falciparum. For example, the work of Wang et al.[44] identified transketolase inhibitors that exhibited similar binding affinities, around -7.5 to -8.0 kcal/mol, suggesting that our synthesized compound is within the range of known effective inhibitors. Furthermore, our observation of competitive inhibition with TPP is supported by studies showing that small molecules with binding affinities below -7.0 kcal/mol are typically strong competitors for active site occupancy.[51]

In contrast to these earlier studies, our compound exhibited a higher affinity than TPP, which suggests it may offer a more robust inhibition mechanism. This finding highlights the potential of the synthesized compound for further optimization and testing as an antimalarial agent, offering an alternative strategy for inhibiting key metabolic pathways in the parasite.

Table 2: Binding Affinity, Polar Interactions, and Distances of Synthesized Compound and Thiamine Pyrophosphate (TPP).

Ligand	Binding Affinity (kcal/mol)	Residues within 4Å of Ligand	Polar Interaction	Bonding Distance
(E)-3a, 8a-dihydroxy-3-((2, 4-hydroxybenzylidene) amino)-2-thioxo-1, 3, 3a, 8a-tetrahydroindeno[1, 2-d] imidazol-8(2H)-one	-7.8	ASN190, LYS191, ILE192, GLU221, ARG250, THR251, ALA252	-COO (side chain) of GLU 221; -OH of benzene moiety of ligand	2.2 Å
Thiamine Pyrophosphate (TPP)	-6.7	HIS31, GLY161, ASP160, ASN190, ILE192, LEU121, GLY159, ASP188	-NH (backbone) of GLY 161; O of phosphate group of pyrrole moiety; NH of HIS31	3.1 Å, 3.2 Å, 1.8 Å, 3.3 Å

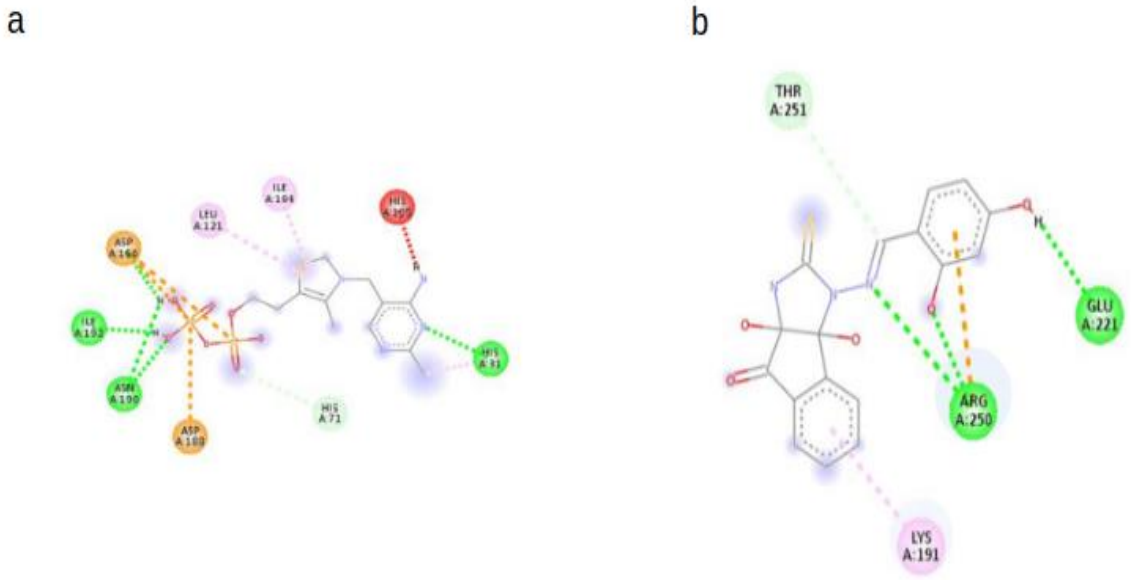

Figure 5: 2D Representations of Protein-Ligand Interactions in Transketolase. a) 2D representation of the interactions between (E)-3a, 8a-dihydroxy-3-((2, 4-hydroxybenzylidene) amino)-2-thioxo-1, 3, 3a, 8a-tetrahydroindeno[1, 2-d] imidazol-8(2H)-one and transketolase. The figure highlights key residues within 4 Å of the ligand, including polar contacts that stabilize the ligand in the enzyme's active site. The compound forms multiple hydrogen bonds with critical residues such as GLU 221 and ARG 250, which are vital for the enzyme's function. b) 2D representation of the interactions between thiamine pyrophosphate (TPP), the natural cofactor of transketolase, and the enzyme. The figure shows the residues within 4 Å of the cofactor, illustrating the hydrogen bonding and other interactions, including bonds with HIS 31, HIS 71, and ASP 160. These interactions are critical for the proper catalytic activity of transketolase.

Molecular Dynamics Simulation

Molecular dynamics (MD) simulations provide valuable insight into the stability, flexibility, and conformational changes of both the protein and ligand complexes over time. In this study, MD simulations were carried out to evaluate the dynamic behavior of the transketolase enzyme complexed with both the synthesized compound (E)-3a, 8a-dihydroxy-3-((2, 4-hydroxybenzylidene) amino)-2-thioxo-1, 3, 3a, 8a-tetrahydroindeno[1, 2-d] imidazol-8(2H)-one and thiamine pyrophosphate (TPP), the natural cofactor. The following sections discuss the results of the root mean square deviation (RMSD), root mean square fluctuation (RMSF), radius of gyration (Rg), and solvent-accessible surface area (SASA) analyses.

Root Mean Square Deviation (RMSD)

The RMSD plot, presented in Figure 6A, reveals the backbone fluctuations for both TPP and the synthesized compound bound to transketolase. The RMSD values provide a measure of the system's stability over the simulation period. Both compounds exhibit relatively stable RMSD values, indicating that the complexes achieved equilibrium early in the simulation and maintained stability throughout the 50-ns timescale.

Notably, the synthesized compound exhibited slightly higher RMSD values compared to TPP, which may indicate a marginally greater degree of flexibility within the transketolase-synthesized compound complex. However, the overall low fluctuations (ranging from 0.2 to 0.5 nm) suggest that both complexes remained stable during the MD simulation. Stability is an important indicator of the reliability of molecular interactions, particularly for potential drug candidates, as it implies strong binding at the protein active site.

Root Mean Square Fluctuation (RMSF)

The RMSF analysis, shown in Figure 6B, provides insights into the flexibility of individual amino acid residues in the transketolase protein. Higher RMSF values correspond to increased flexibility, which may indicate regions of the protein involved in dynamic interactions or loop regions. The RMSF plot highlights several regions with elevated fluctuations, suggesting localized flexibility, particularly around the loops and binding sites.

Both the synthesized compound and TPP exhibited fluctuations in similar regions of the enzyme, with notable peaks at key residues involved in ligand interactions. The fact that both ligands show similar RMSF patterns suggests that the synthesized compound may be binding to the enzyme in a manner similar to TPP. However, the synthesized compound showed slightly elevated fluctuations in some regions, which could reflect differences in the binding mode or dynamics of interaction compared to the natural cofactor.

Radius of Gyration (Rg)

The Rg plot, depicted in Figure 6C, provides a measure of the overall compactness of the protein-ligand complexes. A lower Rg value indicates that the protein structure is more compact, while higher Rg values suggest a less compact, more extended structure. The Rg values for both TPP and the synthesized compound complexes remained relatively stable over the course of the simulation, with TPP displaying slightly lower Rg values compared to the synthesized compound.

The more compact structure of the TPP complex may indicate tighter binding and better structural integrity, which is expected given its role as the natural cofactor. On the other hand, the synthesized compound still exhibited a stable and consistent Rg value, suggesting that its binding did not induce significant structural destabilization, and it maintained relatively strong interactions with transketolase.

Solvent Accessible Surface Area (SASA)

The SASA plot in Figure 6D measures the extent of solvent exposure of the residues in the protein-ligand complexes. Increased solvent exposure can affect the stability of a complex, with lower SASA values generally indicating better buried and stabilized ligands. The synthesized compound demonstrated a higher SASA value compared to TPP, suggesting that it has greater solvent exposure.

Although higher SASA values might imply a less tightly bound complex, this does not necessarily undermine the potential of the synthesized compound as an inhibitor. The increased solvent exposure could be due to differences in ligand size and conformation, and it may allow the compound to make additional water-mediated contacts that could enhance its inhibitory potential.

Free Energy of Binding Decomposition

The free energy binding decomposition analysis, illustrated in Figure 6E, breaks down the total binding free energy into different components, including van der Waals (VDWAALS), electrostatic (EEL), and polar solvation (GSOLV) contributions. As shown in the plot, the synthesized compound exhibited a favorable total binding energy compared to TPP, particularly in terms of electrostatic and van der Waals contributions.

The favorable electrostatic interactions, combined with strong van der Waals forces, suggest that the synthesized compound forms energetically favorable contacts with the transketolase enzyme. These findings further support the potential of the synthesized compound as a competitive inhibitor of transketolase, offering a promising strategy for antimalarial drug development.

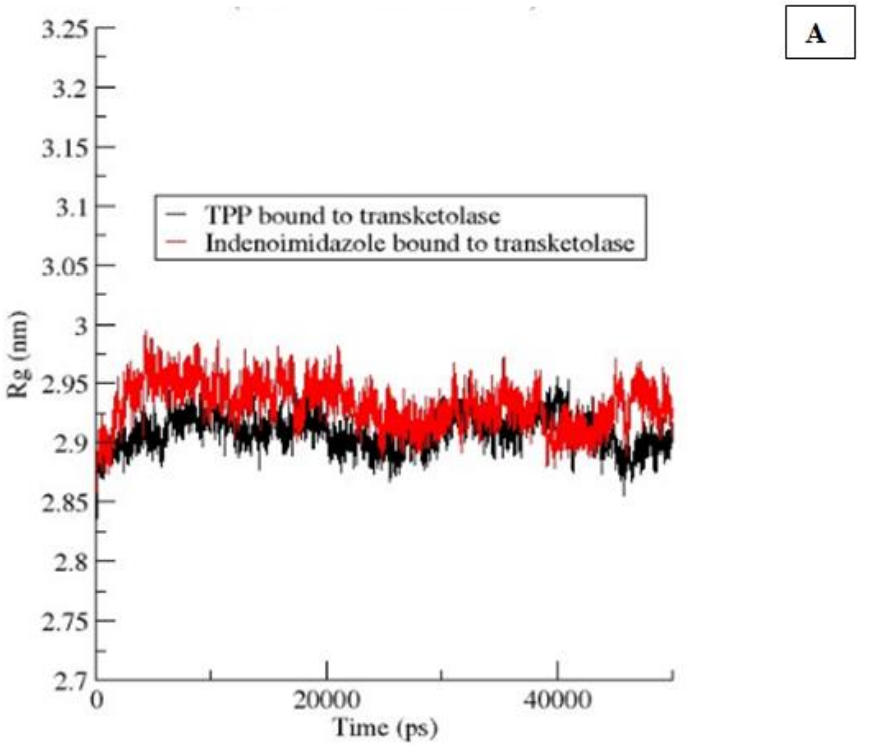
A
TPP bound to transketolase
Indenoimidazole bound to transketolase
Rg (nm)
3.25
3.2
3.15
3.1
3.05
3
2.95
2.9
2.85
2.8
2.75
2.7
0
20000
40000
Time (ps)

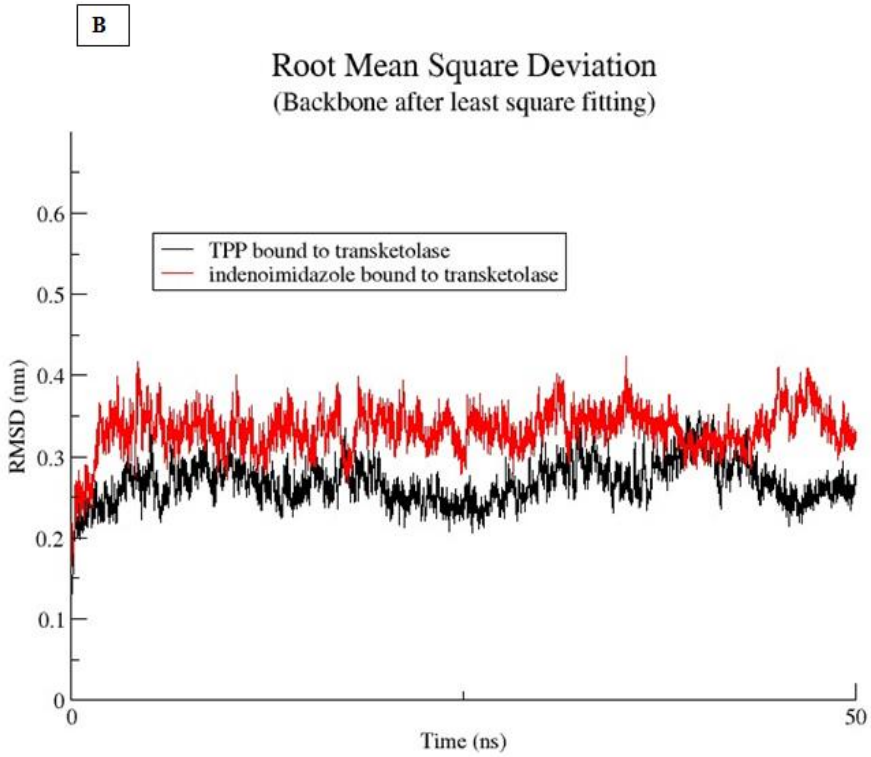
B
Root Mean Square Deviation
(Backbone after least square fitting)
TPP bound to transketolase
indenoimidazole bound to transketolase
RMSD (nm)
0.6
0.5
0.4
0.3
0.2
0.1
0
0
50
Time (ns)

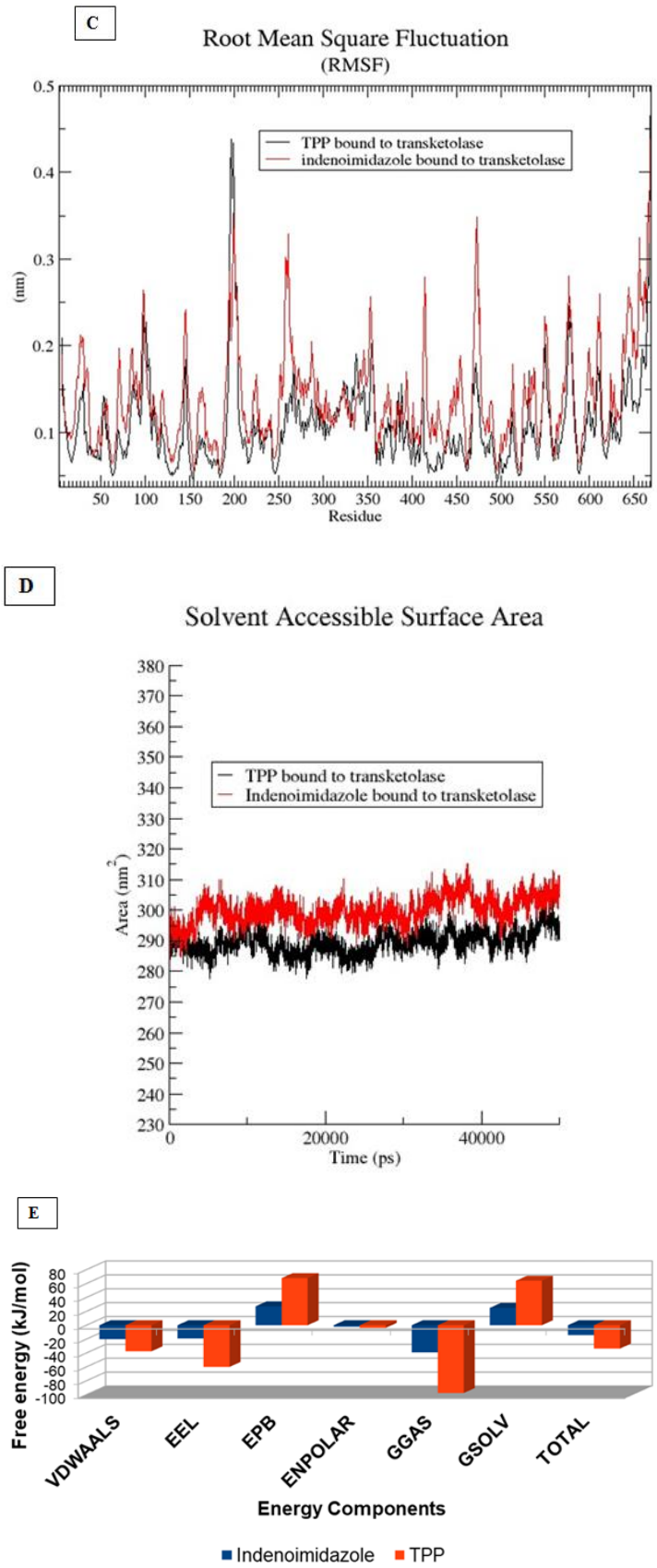

Figure 6: Comparative Analysis of Molecular Dynamics Simulations for Transketolase-Ligand Complexes/ A) Root Mean Square Deviation (RMSD) Plot: the RMSD values of the transketolase backbone when bound to both the synthesized compound *(E)-3a, 8a-dihydroxy-3-((2, 4-hydroxybenzylidene) amino)-2-thioxo-1, 3, 3a, 8a-tetrahydroindeno[1, 2-d] imidazol-8(2H)-one* (red line) and its natural cofactor thiamine pyrophosphate (TPP,

black line). The plot shows the stability of the enzyme-ligand complexes over a 50 ns simulation. RMSD values were calculated after least-square fitting to determine the overall backbone stability, indicating minimal deviation and sustained equilibrium during the simulation. B) Root Mean Square Fluctuation (RMSF) Plot: the RMSF plot represents the flexibility of the individual residues in the transketolase protein over the course of the simulation for both the synthesized compound and TPP. Peaks in the plot correspond to regions of the protein that exhibit higher flexibility. This analysis highlights fluctuations, particularly in loop regions and binding pockets, demonstrating differences in residue mobility between the two complexes. C) Radius of Gyration (Rg) Plot: the Rg plot compares the compactness of the transketolase protein when bound to the synthesized compound (red) and TPP (black). Rg provides a measure of the protein's spatial distribution over time. Lower Rg values for TPP suggest a slightly more compact structure, but both complexes maintained consistent structural integrity throughout the simulation. D) Solvent Accessible Surface Area (SASA) Plot: the solvent exposure of transketolase residues in the presence of the synthesized compound and TPP over the course of the molecular dynamics simulation. The higher SASA value for the synthesized compound indicates greater solvent exposure, possibly due to differences in ligand size and binding conformation, while TPP demonstrated slightly lower solvent interaction. E) Free Energy Binding Decomposition: the bar graph displays the different energy components (VDWAALS, EEL, EPB, ENPOLAR, GGAS, GSOLV) contributing to the binding affinity of both the synthesized compound and TPP. The plot demonstrates the contributions of van der Waals forces, electrostatic interactions, and solvation effects to the overall binding energy. The synthesized compound exhibited favorable binding free energy due to its strong electrostatic and van der Waals interactions, further supporting its potential as a competitive inhibitor of transketolase.

Pharmacological Efficacy of the Synthesized Compound on Parasitemia and Chemosuppression

The pharmacological efficacy of the synthesized compound, (E)-3a, 8a-dihydroxy-3-((2, 4-hydroxybenzylidene) amino)-2-thioxo-1, 3, 3a, 8a-tetrahydroindeno [1, 2- d] imidazol-8(2H)-one, was evaluated in a mouse model infected with Plasmodium berghei. The results of parasitemia and chemosuppression percentages demonstrate the compound's antimalarial potential compared to chloroquine (CQ), a standard antimalarial drug. As shown in Figure 7a, the control group displayed high parasitemia levels, indicative of an unchecked infection, while all treatment groups exhibited significant reductions in parasitemia levels, underscoring the efficacy of both CQ and the synthesized compound.

The survival index, as shown in Figure 7c, further validates the potential of the synthesized compound as an antimalarial agent. While chloroquine achieved a survival index of 68.97%, the synthesized compound achieved a remarkable 100% survival rate at 25 mg/kg, indicating that the compound not only reduces parasitemia but also significantly improves survival outcomes in infected mice. However, at lower doses (5 mg/kg and 10 mg/kg), the survival index of the synthesized compound was lower (39.66% and 24.14%, respectively), despite the high chemosuppression observed at these doses (78.07% and 83.55%, respectively). This discrepancy suggests that while the compound effectively reduces parasitemia, its therapeutic effect on overall survival may require higher dosages for maximal efficacy.

This pattern aligns with previous studies on other antimalarial compounds, where survival outcomes were closely linked to the ability of the drug to maintain parasite suppression over time.[52] Additionally, the high survival rate at 25 mg/kg suggests that the synthesized compound could be an effective alternative or complement to existing antimalarial treatments, especially in scenarios of chloroquine resistance.[53]

The observed chemosuppressive activity of the synthesized compound indicates its potential to interfere with the life cycle of the malaria parasite, likely by disrupting its ability to replicate within red blood cells. The higher chemosuppression at 25 mg/kg could be explained by the compound's interaction with key metabolic pathways in Plasmodium berghei, inhibiting the synthesis of vital components necessary for the parasite's survival and replication.[54] This mode of action could be analogous to that of chloroquine, which is known to interfere with the parasite's ability to detoxify hemoglobin.[55] The results of this study suggest that the synthesized compound may act on similar biochemical pathways, though further molecular studies are required to elucidate its precise mechanism of action.

The lower survival indices observed at 5 mg/kg and 10 mg/kg indicate that, while the compound effectively reduces parasitemia, it may not provide sufficient therapeutic benefit at these doses to ensure prolonged survival. This could be due to the pharmacokinetic properties of the compound, where higher concentrations are required to maintain therapeutic levels in the bloodstream and tissues for extended periods.[56] The sharp increase in survival index at 25 mg/kg suggests that once a threshold concentration is achieved, the compound's efficacy is markedly enhanced, resulting in both effective parasitemia control and improved survival outcomes.

Chloroquine, despite being a widely used antimalarial drug, has shown reduced efficacy in many malaria-endemic regions due to the emergence of drug-resistant strains of *Plasmodium falciparum*.[57] In this study, the synthesized compound demonstrated a more favorable

profile in terms of parasitemia reduction and survival enhancement, especially at higher doses. The lower parasitemia and higher chemosuppression observed with the synthesized compound, even at doses as low as 5 mg/kg, indicate that it may have a distinct advantage over chloroquine in terms of potency and potential to overcome resistance mechanisms.

The synthesized compound's superior chemosuppression and survival outcomes at 25 mg/kg highlight its promise as a candidate for further development. However, the lower survival indices at lower doses suggest that optimization of dosing regimens or formulation improvements may be necessary to maximize its clinical potential. Given that chloroquine-resistant malaria strains are an ongoing global health challenge, the development of novel antimalarial agents such as this synthesized compound is of utmost importance.[58]

The promising results from this study pave the way for further research into the pharmacokinetics, safety, and long-term efficacy of the synthesized compound. Future studies could focus on expanding the in vivo model to include other malaria strains, such as *Plasmodium falciparum*, to determine whether the compound's efficacy extends beyond *Plasmodium berghei*.[59] Moreover, molecular docking and simulation studies could be employed to investigate the interaction of the compound with key parasitic enzymes and pathways, providing further insight into its mechanism of action.[60]

The synthesized compound shows significant potential as an antimalarial agent, demonstrating superior chemosuppressive activity and survival benefits compared to chloroquine. While the compound's efficacy at lower doses may require further optimization, its performance at higher doses suggests that it could serve as a valuable alternative or complement to existing malaria therapies.

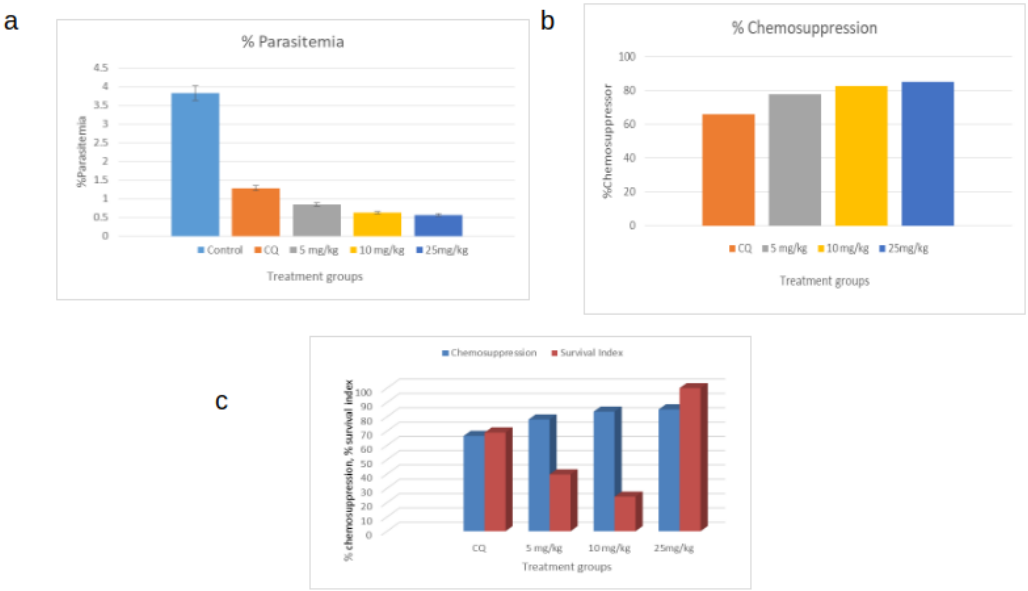

Figure 7: Antimalarial Efficacy of (E)-3a, 8a-Dihydroxy-3-((2, 4-Hydroxybenzylidene) Amino)-2-Thioxo-1, 3, 3a, 8a-Tetrahydroindeno [1, 2-d] Imidazol-8(2H)-one and Chloroquine against Plasmodium berghei in Mice. a) Parasitemia Levels in Mice: This bar chart represents the percent parasitemia in mice infected with Plasmodium berghei and treated with different doses of chloroquine (CQ) and the synthesized compound (E)-3a, 8a-dihydroxy-3-((2, 4-hydroxybenzylidene) amino)-2-thioxo-1, 3, 3a, 8a-tetrahydroindeno[1, 2-d] imidazol-8(2H)-one. The compound shows a dose-dependent reduction in parasitemia, with the highest efficacy observed at 25 mg/kg. Values are expressed as mean ± SD (n=5, $p<0.05$). b) Chemosuppression of Parasitemia: The percentage of chemosuppression achieved by chloroquine and the synthesized compound at different doses is depicted. Both agents demonstrate significant chemosuppression, with the synthesized compound achieving higher suppression levels than chloroquine, particularly at higher doses. c) Chemosuppression and Survival Index in Mice: The graph shows a comparison between chemosuppression and survival index in Plasmodium berghei-infected mice treated with chloroquine and different doses of the synthesized compound. While chemosuppression was high across all doses, the survival index was notably lower at 5 mg/kg and 10 mg/kg for the synthesized compound, indicating suboptimal therapeutic advantage at these doses. However, the 25 mg/kg dose showed a survival index of 100%, surpassing chloroquine and demonstrating strong potential for further antimalarial studies.

CONCLUSION

This study successfully synthesized and characterized a novel indenoimidazole derivative, (E)-3a, 8a-dihydroxy-3-((2,4-hydroxybenzylidene) amino)-2-thioxo-1,3,3a,8a-tetrahydroindeno [1,2-d] imidazol-8(2H)-one, which demonstrated significant antimalarial potential by

targeting the enzyme transketolase in *Plasmodium berghei*. Molecular docking and dynamics simulations confirmed a strong and stable interaction between the compound and transketolase, with superior binding affinity compared to the natural cofactor thiamine pyrophosphate. In vivo pharmacological evaluation showed high chemosuppressive activity, reducing parasitemia by 85.12% at a dose of 25 mg/kg, and achieving a 100% survival index in the treated mice. These results suggest that the synthesized compound has promising potential as a new antimalarial agent, particularly in the face of growing resistance to existing therapies like chloroquine. Further optimization and investigation into its efficacy against other resistant malaria strains, as well as detailed studies on its pharmacokinetic and safety profiles, are warranted to establish its clinical viability.

REFERENCES

1. World Health Organization. (2022). World Malaria Report. http://www.who.int/malaria/publications/worldmalariareport/en/
2. Punsawad, C., Viriyavejakul, P. (Reduction in serum sphingosine 1-phosphate concentration in malaria). PLOS ONE, 2017; 12(6): e0180631. doi.org/10.1371/journal.pone.0180631
3. Boutayeb, A. The impact of infectious diseases on the development of Africa. In V.R. Preedy and R.R. Watson (eds.), Handbook of Disease Burdens and Quality of Life Measures. New York, NY: Springer New York. 2022; 1171 –1188. doi.org/10.1007/978-0-387-78665-0_66
4. Sinha, S., Medhi, B., Sehgal, R. (Challenges of drug-resistant malaria). Parasite, 2014; 21: 61. doi.org/10.1051/parasite/2014059
5. Basco, L. K., Ringwald, P. (Chloroquine resistance in Plasmodium falciparum and polymorphism of the CG2 gene). Journal of Infectious Diseases, 1999; 180(6): 1979 - 1986. doi:10.1086/315140
6. Miotto O., Amato R., Dance DAB., MacInnis B., Almagro-Garcia J., Amaratunga C., Kwiatkowski DP. (Genetic Architecture of Artemisinin-resistant Plasmodium Falciparum). Nature Genetics, 2015; 47(3): 226-234. doi.org/10.1038/ng.3189
7. Stincone A, Prigione, A, Cramer T., Wamelink, MMC., Campbell K, Cheung E., Olin-Sandoval V., et al.. (The return of metabolism: Biochemistry and physiology of the pentose phosphate pathway). Biological Reviews, 2015; 90(3): 927–963. doi.org/10.1111/brv.12140
8. Ramsden CA., Katritzky, AR., Scriven EFV, Taylor RJK. Comprehensive Heterocyclic Chemistry III: A Review of the Literature 2008–2009. Elsevier.
9. Zhang C., Zhang Z., Zhu Y., Qin S. (Glucose-6-phosphate dehydrogenase: A biomarker and potential therapeutic target for cancer). Anticancer Agents in Medicinal Chemistry, 2014; 14(2): 280–289.
10. Tolomeu H.V., Fraga CAM. (Imidazole: Synthesis, functionalization and physicochemical properties of a privileged structure in medicinal chemistry. Molecules (Basel, Switzerland)), 2023; 28(2): 838. doi.org/10.3390/molecules28020838
11. Shaker B., Ahmad S., Lee J., Jung C., Na D. (In silico methods and tools for drug discovery). Computers in Biology and Medicine, 2021; 137: 104851.
12. Liu X., Shi D., Zhou S., Liu H., Liu H., Yao X. (Molecular dynamics simulations and novel drug discovery). Expert Opinion on Drug Discovery, 2018; 13(1): 23-37. doi.org/10.1080/17460441.2018.1403419
13. Chen G., Seukep A.J., Guo M. (Recent advances in molecular docking for the research and discovery of potential marine drugs). Marine Drugs, 2020; 18(11): 545. doi.org/10.3390/md18110545
14. Sali A., Blundell TL. (Comparative protein modelling by satisfaction of spatial Restraints). J Mol Biol, (1993); 234: 779-815.
15. Abraham MJ, Murtola T, Schulz R, Páll S, Smith JC, Hess B, Lindahl E. (GROMACS: High performance molecular simulations through multi-level parallel is from laptops to supercomputers). SoftwareX, 2015; 1-2: 19-25. doi.org/10.1016/j.softx.2015.06.001
16. Morris GM, Huey R, Lindstrom W, Sanner MF, Belew RK, Goodsell DS, Olson AJ. (AutoDock4 and AutoDockTools4: automated docking with selective receptor flexibility). J Comput Chem., 2009; 30(16): 2785-2791. doi.org/10.1002/jcc.21256
17. Trott O, Olson AJ. (AutoDock Vina: improving the speed and accuracy of docking with a new scoring function, efficient optimization and multithreading). J Comput Chem., 2010; 31: 455-461.
18. Marsh J, Teichmann S. (Relative solvent accessible surface area predicts protein conformational changes upon binding). Structure, 2011; 19: 859-867. doi.org/10.1016/j.str.2011.03.010
19. Kumari R, Kumar R. (Open Source Drug Discovery Consortium, Lynn A. g_mmpbsa–a GROMACS tool for high-throughput MM PBSA calculations). J Chem Inf Model, 2014; 54(7): 1951-1962. doi.org/10.1021/ci500020m
20. Pant R, Joshi A, Maiti P, Nand M., Pande V, Chandra S. (Identification of potential mycolyltransferase Ag85C inhibitors of Mycobacterium tuberculosis H37Rv via virtual High Throughput Screening and binding free energy studies). J Mol Graph Model, 2020. doi.org/10.1016/j.jmgm.2020.107584
21. Lorke D. (A new approach to tropical acute toxicity testing). Arch Toxicol, 1983; 53: 275-285.
22. Knight DJ, Peters W. (The antimalarial activity of N-benzyloxydihydrotriazines. I. The activity of clociguanil (BRL 50216) against rodent malaria, and studies on its mode of action). Ann Trop Med Parasitol, 1980; 74: 393–404.
23. Mengiste B, Makonnen E, Urga K. (In vivo antimalarial activity of Dodonaea Angustifolia seed

extracts against Plasmodium berghei in mice model). Momona Ethiopian Journal of Science, 2012; 4(1): 47-63.
24. Sweeney M, Conboy D, Mirallai SI, Aldabbagh F. (Advances in the Synthesis of Ring-Fused Benzimidazoles and Imidazobenzimidazoles). Molecules, 2021; 26(9): 2684. https://doi.org/10.3390/molecules26092684
25. Chandy S K, Krishnan Raghavachari. (Accurate and Cost-Effective NMR Chemical Shift Predictions for Nucleic Acids Using a Molecules-in-Molecules Fragmentation-Based Method). Journal of Chemical Theory and Computation, 2023; 19(2): 544–561. https://doi.org/10.1021/acs.jctc.2c00967
26. Georgieva MK, Anastassova N, Denitsa Stefanova, Denitsa Yancheva. (Radical Scavenging Mechanisms of 1-Arylhydrazone Benzimidazole Hybrids with Neuroprotective Activity). The Journal of Physical Chemistry B., 2023; 127(20): 4364–4373. https://doi.org/10.1021/acs.jpcb.2c05784
27. Singh G, Gupta D. (In-Silico Functional Annotation of Plasmodium falciparum Hypothetical Proteins to Identify Novel Drug Targets). Frontiers in Genetics, 2022; 13. https://doi.org/10.3389/fgene.2022.821516
28. Boateng RA, Tastan Bishop Ö., Musyoka TM. (Characterisation of plasmodial transketolases and identification of potential inhibitors: an in silico study). Malaria Journal, 2020; 19(1). https://doi.org/10.1186/s12936-020-03512-1
29. Jia D, Liu C, Zhu Z, Cao Y, Wen W, Hong Z, Liu Y, Liu E, Chen L, Chen C, Gu Y, Jiao B, Chai Y, Wang H, Fu J, Chen X. (Novel transketolase inhibitor oroxylin A suppresses the non-oxidative pentose phosphate pathway and hepatocellular carcinoma tumour growth in mice and patient-derived organoids). Clinical and Translational Medicine, 2022; 12(11). https://doi.org/10.1002/ctm2.1095
30. Wu PS, Enervald E, Joelsson A, Palmberg C, Rutishauser D, Hällberg BM, Ström L. (Post-translational Regulation of DNA Polymerase η, a Connection to Damage-Induced Cohesion in *Saccharomyces cerevisiae*). Genetics, 2020; 216(4): 1009–1022. https://doi.org/10.1534/genetics.120.303494
31. Jones D, Kim H, Zhang X, Zemla A, Stevenson G, Bennett WF, Kirshner D, Wong SE, Lightstone FC, Allen JE. (Improved Protein–Ligand Binding Affinity Prediction with Structure-Based Deep Fusion Inference). Journal of Chemical Information and Modeling, 2021; 61(4): 1583–1592. https://doi.org/10.1021/acs.jcim.0c01306
32. Postic G, Janel N, Tufféry P, Moroy G. (An information gain-based approach for evaluating protein structure models). Computational and Structural Biotechnology Journal, 2020; 18: 2228–2236. https://doi.org/10.1016/j.csbj.2020.08.013
33. Boutayeb A. The impact of infectious diseases on the development of Africa. In: V.R. Preedy & R.R. Watson (eds.), Handbook of Disease Burdens and Quality of Life Measures, 1171–1188. New York, NY: Springer New York. doi.org/10.1007/978-0-387-78665-0_66
34. Gökçe Uludoğan, Elif Ozkirimli, Ulgen K. O, Nilgün Karalı, Arzucan Özgür. (Exploiting pretrained biochemical language models for targeted drug design). Bioinformatics, 2022; 38(2): 155–161. https://doi.org/10.1093/bioinformatics/btac482
35. Audrone Valanciute, Nygaard, L., Henrike Zschach, Michael Maglegaard Jepsen, Kresten Lindorff-Larsen, & Stein, A. Accurate protein stability predictions from homology models. *Computational and Structural Biotechnology Journal*, 2023; *21:* 66–73. https://doi.org/10.1016/j.csbj.2022.11.048
36. Muegge, I., & Hu, Y. Recent Advances in Alchemical Binding Free Energy Calculations for Drug Discovery. *ACS Medicinal Chemistry Letters*, 2023; *14*(3): 244–250. https://doi.org/10.1021/acsmedchemlett.2c00541
37. King, E., Aitchison, E., Li, H., & Luo, R. Recent Developments in Free Energy Calculations for Drug Discovery. *Frontiers in Molecular Biosciences*, 2021; *8*. https://doi.org/10.3389/fmolb.2021.712085
38. Sobolev, O. V., Afonine, P. V., Moriarty, N. W., Hekkelman, M. L., Joosten, R. P., Anastassis Perrakis, & Adams, P. D. (2020). A global Ramachandran score identifies protein structures with unlikely stereochemistry. *BioRxiv (Cold Spring Harbor Laboratory)*. https://doi.org/10.1101/2020.03.26.010587
39. Carrascoza, F., Antczak, M., Miao, Z., Westhof, E., & Szachniuk, M. Evaluation of the stereochemical quality of predicted RNA 3D models in the RNA-Puzzles submissions. *BioRxiv (Cold Spring Harbor Laboratory)*, 2021. https://doi.org/10.1101/2021.08.22.457258
40. Bhattacharjee, K., Soundhararajan Gopi, & Naganathan, A. N. A Disordered Loop Mediates Heterogeneous Unfolding of an Ordered Protein by Altering the Native Ensemble. *The Journal of Physical Chemistry Letters*, 2020; *11*(16): 6749–6756. https://doi.org/10.1021/acs.jpclett.0c01848
41. Fiorentini, R., Kremer, K., & Potestio, R. Ligand-protein interactions in lysozyme investigated through a dual-resolution model. *Proteins: Structure, Function, and Bioinformatics*, 2020; *88*(10): 1351–1360. https://doi.org/10.1002/prot.25954
42. Xia, N., Guo, X., Guo, Q., Gupta, N., Ji, N., Shen, B., Xiao, L., & Feng, Y. Metabolic flexibilities and vulnerabilities in the pentose phosphate pathway of the zoonotic pathogen Toxoplasma gondii. *PLoS Pathogens*, 2022; *18*(9): e1010864–e1010864. https://doi.org/10.1371/journal.ppat.1010864
43. Sirous, H., Campiani, G., Calderone, V., & Brogi, S. Discovery of novel hit compounds as potential HDAC1 inhibitors: The case of ligand- and structure-based virtual screening. *Computers in Biology and Medicine*, 2021; *137:* 104808. https://doi.org/10.1016/j.compbiomed.2021.104808
44. Wang, Y., Yang, F., Yan, D., Zeng, Y., Wei, B., Chen, J., & He, W. Identification Mechanism of

BACE1 on Inhibitors Probed by Using Multiple Separate Molecular Dynamics Simulations and Comparative Calculations of Binding Free Energies. *Molecules*, 2023; *28*(12): 4773–4773. https://doi.org/10.3390/molecules28124773

45. Oladejo, D. O., Oduselu, G. O., Dokunmu, T. M., Isewon, I., Oyelade, J., Okafor, E., Iweala, E. E., & Adebiyi, E. *In silico* Structure Prediction, Molecular Docking, and Dynamic Simulation of *Plasmodium falciparum* AP2-I Transcription Factor. *Bioinformatics and Biology Insights*, 2023; *17:* 117793222211496. https://doi.org/10.1177/11779322221149616
46. Tsebriy, O., Khomiak, A., Miguel-Blanco, C., Sparkes, P. C., Gioli, M., Santelli, M. Whitley, E., Gamo, F.-J., & Delves, M. J. *Machine Learning-based Phenotypic Imaging to Characterise the Targetable Biology of*Plasmodium falciparum*Male Gametocytes for the Development of Transmission-Blocking Antimalarials*, 2023. https://doi.org/10.1101/2023.04.22.537818
47. Dickie, E. A., Ronin, C., Sá, M., Ciesielski, F., Trouche, N., Tavares, J., Santarem, N., Major, L. L., Pemberton, I. K., MacDougall, J., Smith, T. K., Cordeiro-da-Silva, A., & Ciapetti, P. Toward Chemical Validation of Leishmania infantum Ribose 5-Phosphate Isomerase as a Drug Target. *Antimicrobial Agents and Chemotherapy*, 2021; *65*(7). https://doi.org/10.1128/aac.01892-20
48. Nauton, L., Hecquet, L., & Thery, V. QM/MM Study of Human Transketolase: Thiamine Diphosphate Activation Mechanism and Complete Catalytic Cycle. *Journal of Chemical Information and Modeling*, 2021; *61*(7): 3502–3515. https://doi.org/10.1021/acs.jcim.1c00190
49. Ali, M., Malik, K., Zaidi, A., Farooq, U., Syed Majid Bukhari, Majeed, Z., Mahnashi, M. H., Shamyla Nawazish, Alqahtani Abdulwahab, & Alshaibari, K. S. In-vitro high-throughput library screening—Kinetics and molecular docking studies of potent inhibitors of α-glucosidase. *PloS One*, 2023; *18*(6): e0286159–e0286159. https://doi.org/10.1371/journal.pone.0286159
50. Jung, Y., Noda, N., Takaya, J., Abo, M., Toh, K., Tajiri, K., Cui, C., Zhou, L., Sato, S., & Uesugi, M. Discovery of Non-Cysteine-Targeting Covalent Inhibitors by Activity-Based Proteomic Screening with a Cysteine-Reactive Probe. *ACS Chemical Biology*, 2022; *17*(2): 340–347. https://doi.org/10.1021/acschembio.1c00824
51. Magwenyane, A. M., Mhlongo, N. N., Lawal, M. M., Amoako, D. G., Somboro, A. M., Sosibo, S. C., Shunmugam, L., Khan, R. B., & Kumalo, H. M. Understanding the Hsp90 N-Terminal Dynamics: Structural and Molecular Insights into the Therapeutic Activities of Anticancer Inhibitors Radicicol (RD) and Radicicol Derivative (NVP-YUA922). *Molecules*, 2020; *25*(8): 1785. https://doi.org/10.3390/molecules25081785
52. Dibessa, T. T., Engidawork, E., Nedi, T., & Teklehaymanot, T. Antimalarial activity of the aqueous extract of the latex of Aloe pirottae Berger. (Aloaceae) against Plasmodium berghei in mice. *Journal of Ethnopharmacology*, 2020; *255:* 112763. https://doi.org/10.1016/j.jep.2020.112763
53. Jaromin, A., Parapini, S., Basilico, N., Zaremba-Czogalla, M., Agnieszka Lewińska, Agnieszka Zagórska, Walczak, M., Bożena Tyliszczak, Grzeszczak, A., Marcin Łukaszewicz, Kaczmarek, Ł., & Jerzy Gubernator. Azacarbazole n-3 and n-6 polyunsaturated fatty acids ethyl esters nanoemulsion with enhanced efficacy against Plasmodium falciparum. *Bioactive Materials*, 2021; *6*(4): 1163–1174. https://doi.org/10.1016/j.bioactmat.2020.10.004
54. Colón-Lorenzo, E. E., Colón-López, D. D., Vega-Rodríguez, J., Dupin, A., Fidock, D. A., Baerga-Ortiz, A., Ortiz, J. G., Bosch, J., & Serrano, A. E. Structure-Based Screening of Plasmodium berghei Glutathione S-Transferase Identifies CB-27 as a Novel Antiplasmodial Compound. *Frontiers in Pharmacology*, 2020; *11*. https://doi.org/10.3389/fphar.2020.00246
55. Parth, Kaur, N., Korkor, C., Mobin, S. M., Chibale, K., & Singh, K. Fluorene-Chloroquine Hybrids: Synthesis, *in vitro* Antiplasmodial Activity, and Inhibition of Heme Detoxification Machinery of *Plasmodium falciparum*. *ChemMedChem*, 2022; *17*(19). https://doi.org/10.1002/cmdc.202200414
56. De Sutter, P.-J., De Cock, P., Johnson, T. N., Musther, H., Gasthuys, E., & Vermeulen, A. Predictive Performance of Physiologically Based Pharmacokinetic Modelling of Beta-Lactam Antibiotic Concentrations in Adipose, Bone, and Muscle Tissues. *Drug Metabolism and Disposition*, 2023; *51*(4): 499–508. https://doi.org/10.1124/dmd.122.001129
57. Sofeu-Feugaing, D. D., Nkengeh Ajonglefac, F., Nyuylam Moyeh, M., Obejum Apinjoh, T., Essende, M. E., Talla Kouam, G. D., & Mbigha Ghogomu, S. Status of the Multidrug Resistance-1 Gene of Plasmodium falciparum in Four Malaria Epidemiological Strata, Two Decades after the Abolition of Chloroquine as First-Line Treatment for Uncomplicated Malaria in Cameroon. *Journal of Tropical Medicine*, 2023; *2023:* 1–9. https://doi.org/10.1155/2023/6688380
58. Wicht, K. J., Mok, S., & Fidock, D. A. Molecular Mechanisms of Drug Resistance in Plasmodium falciparum Malaria. *Annual Review of Microbiology*, 2020; *74*(1): 431–454. https://doi.org/10.1146/annurev-micro-020518-115546
59. Sadeghi, S., Valadkhani, Z., Tafreshi, A. S., Arjmand, M., Nahravanian, H., Vahabi, F., Soori, N., Mohammadi, M., Meigooni, M., & Zamani, Z. A Study of Synergy of Combination of Eosin B with Chloroquine, Artemisinin, and Sulphadoxine-Pyrimethamine on Plasmodium falciparum In Vitro and *Plasmodium berghei* In Vivo. *Journal of*

Tropical Medicine, 2020; *2020:* 1–10. https://doi.org/10.1155/2020/3013701

60. Vidhya, V. M., & Ponnuraj, K. Structure-based virtual screening and computational study towards identification of novel inhibitors of hypoxanthine-guaninephosphoribosyltransferase of *Trypanosoma cruzi*. *Journal of Cellular Biochemistry*, 2021; *122*(11): 1701–1714. https://doi.org/10.1002/jcb.30122